Rare Metal Materials and Engineering
Volume 49, Issue 4, April 2020
Available online at www.rmme.ac.cn

Science Press

Cite this article as: Rare Metal Materials and Engineering, 2020, 49(4): 1119-1125.

ARTICLE

Synthesis of Manganese-Doped TiO_2 Nanosheet as Cathode Catalyst for Rechargeable Li–O_2 Batteries with High Performance

Wang Hongjiao, Wang Hui, Cao Huiqun, Luo Zhongkuan, Wang Fang

Shenzhen University, Shenzhen 518060, China

Abstract: We proposed that Mn-doped TiO_2 nanosheets (Mn-TiO_2 NS) as cathode catalyst improved the electrochemical performance of lithium-air batteries. Firstly, rutile Mn-TiO_2 NS were calcined by a facile hydrothermal treatment method. Secondly, polyvinylidene fluoride (PVDF) was dissolved in an N-methyl-2-pyrrolidone (NMP) solvent. KB and Mn-TiO_2 NS were mixed with a PVDF/NMP solution to fabricate a cathode slurry. Lastly, the cathode slurry was coated onto circular carbon paper (diameter=15 mm) and dried at 60 °C for 3 h in the oven to obtain the air cathode. As expected, lithium-air cells based on KB and Mn-TiO_2 NS electrode exhibit an improved overpotential of 1.24 V and a high discharge capacity of 9374.23 $mAh \cdot g^{-1}$ at the current density of 250 $mA \cdot g^{-1}$. It suggests that Mn-TiO_2 NS is a promising catalyst for Li-O_2 batteries.

Key words: Mn-TiO_2 NS; catalysts effect; KB; high-performance; Li-O_2 batteries

With the deterioration of environment and the depletion of traditional fossil fuel, the development of renewable energy is the general trend of the future. Rechargeable Li-O_2 batteries possess advantages of being a next-generation battery system, due to a similar theoretical specific energy density (11680 $Wh \cdot kg^{-1}$) to gasoline (13000 $Wh \cdot kg^{-1}$)[1-4]. Despite remarkable progress in lithium-air batteries, there still exists great challenges to realize its high-rate and long-term cycling performance, such as low round-trip efficiency, high discharging and charging overpotential and poor cycle stability[5,6]. All of the issues are inherently linked to the sluggish kinetics of oxygen reduction reaction (ORR) and the oxygen evolution reaction (OER). Therefore, it is vital and urgent to improve the kinetics of ORR and OER. So developing efficiently catalysts are one of the keys to achieve high performance Li-O_2 batteries, such as carbon materials[7-10], transition metal oxides[11-17] and precious metals[18-20]. Among the reported cathode catalysts, transition metal oxides have received great attention due to their defective structure, low cost, and catalytic ability.

Recently, TiO_2 was reported as catalyst substrates[21,22], and effective catalysts[23, 24] for Li-O_2 batteries due to its excellent chemical stability. Zhang et al[22] investigated TiO_2 nanotubes as a support for electrocatalysts (RuO_2 and Pt). Agyeman et al[1] demonstrated that TiO_2 could reduce the side reactions and electrolyte decomposition to improve cycle life of a Li-O_2 batteries. In the present paper, it was proposed that Mn-doped TiO_2 nanosheets (Mn-TiO_2 NS) prepared by simple hydrothermal method improved ORR/OER overpotential, discharge capacity and cycling stability for Li-O_2 batteries.

1 Experiment

TiO_2 nanospheres were prepared through a typical sol-gel process. Firstly, 20 mL of anhydrous ethanol (>99.7%, Sigma-Aldrich) and 0.1 mL of KCl (≥99.0%, Aladdin Industrial) solution (0.1 mol/L) were mixed, which were marked as solution A. Then, 0.2 g hexadecylamine (HDA, 98%, Sigma-Aldrich) was dissolved in solution A to prepare solution B. After that, 0.5 mL of titanium (IV) isopropoxide (TIP, >97%, Sigma-Aldrich) was added drop by drop to solution B under 1000 r/min stirring for 2 min to make a white suspension and

Received date: May 9, 2019
Foundation item: Shenzhen Science and Technology Fund (JCYJ20170818095803319)
Corresponding author: Wang Fang, Professor, College of Chemistry and Environmental Engineering, Shenzhen University, Shenzhen 518060, P. R. China, Tel: 0086-755-26557381, E-mail: wangfsz@szu.edu.cn

kept static for 18 h. The precipitation in the white suspension was filtered and washed by anhydrous ethanol three times, and then it was dried in air at 40 °C to prepare TiO_2 particles (TiO_2 PS). Secondly, 0.1 g of as-prepared TiO_2 PS was transferred to a Teflon-lined stainless-steel autoclave filled with the solution which consists of 20 mL of anhydrous ethanol, 17 mL of ammonium hydroxide (25%~28%, Xilong Chemical) and 3 mL of deionized water. After that, the sealed autoclave was put in an electric oven at 130 °C for 72 h. The obtained products are TiO_2 nanosheets (TiO_2 NS), which was transferred from cooled autoclave, and washed with deionized water and the pH was adjusted to 6 by rinsing with diluted HNO_3 solution. After that, the Mn ions were doped into TiO_2 NS via dissolving TiO_2 NS into 200 mL of manganese nitrate tetrahydrate (98%, Alfa Aesar) solution (0.09 mol/L) under constant stirring for 2 h. And then, the excess Mn ions were washed out by deionized water and dried in air at 60 °C. Finally, the prepared Mn-doped TiO_2 nanosheets were obtained (Mn-TiO_2 NS).

The morphology and structure of the TiO_2 PS, TiO_2 NS and Mn-TiO_2 NS were observed by field emission scanning electron microscope (FESEM, JEOL JSM-7800F) and energy dispersive analysis of X-rays (EDS) analysis. The crystal structure of TiO_2 PS, TiO_2 NS and Mn-TiO_2 NS were studied by X-ray diffraction (XRD, Bruker AXS D8 ADVANCE). The effect of dopant was investigated by Raman spectroscopy (HORIBA LabRAM HR 800) and X-ray photoelectron spectroscopy (XPS, Thermo Fisher Scientific Microlab350). The surface area properties were determined by N_2 adsorption/desorption (BELSORP, Bel Japan, Inc.). All the samples were degassed for 3 h at 300 °C under vacuum before surface area measurements.

CR 2032-type coin cells with a plural of Φ=1 mm holes on the cathode cap were assembled in a glove box under an Ar atmosphere with O_2 and H_2O less than 0.5 μL/L using a lithium metal foil anode, a glass fiber separator, an oxygen cathode and an electrolyte containing 1 mol/L lithium bis (trifluoromethanesulfonyl) imide (LiTFSI) in tetraethylene glycol dimethyl ether (TEGDME). The as-fabricated Mn-TiO_2 NS (Φ15 mm) were used as O_2 cathodes for the Li-O_2 cells. For comparison, the carbon cathodes pure KB, KB+TiO_2 PS and KB+TiO_2 NS were prepared by casting a mixture of KB (Ketjin Black) and TiO_2 PS, TiO_2 NS and Mn-TiO_2 NS catalyst, as well as PVDF with a total mass ratio of 9:0:1 and 6:3:1 on a carbon paper (HCP120, Shanghai Hesen Electric) current collector and dried at 60 °C to form the air cathode (TiO_2 PS, TiO_2 NS electrodes and Mn-TiO_2 NS electrode).

In order to compare the stabilities of the four electrodes, the galvanostatic discharge-charge tests were conducted within a voltage window of 2.2~4.4 V with a multichannel battery testing system (LAND CT 2001A) in a testing dry air circumstance box (dried by silica gel and calcium oxide, 25 °C controlled by air-conditioner). Cyclic voltammetry (CV) and A.C. impedance tests were carried out by an electrochemical workstation (CHI660D). The A.C. impedance spectra were recorded in a frequency range from100 kHz to 0.1 Hz.

2 Results and Discussion

2.1 Physical and chemical characterizations of catalysts

The morphologies of the as-prepared TiO_2 PS, TiO_2 NS and Mn-TiO_2 NS are shown in Fig.1. It can be seen in Fig.1a that the particle is typically spherical. After the hydrothermal and calcination processes, the TiO_2 particles (TiO_2 PS) are transformed into TiO_2 nanosheets (TiO_2 NS) in Fig.1b. Additionally, it is seen in Fig.1c that the morphology of Mn-TiO_2 NS is similar to that of TiO_2 NS. In order to further find out the amount of Mn, TiO_2 NS and Mn-TiO_2 NS, samples were analyzed by EDS (Fig.2a and 2b). As shown in Fig.2b and Table 1, Ti peaks, O peaks and Mn peaks are detected, which implies the existence of Mn element.

The XRD results of the TiO_2 PS, TiO_2 NS and Mn-TiO_2 NS are presented in Fig.3. All of the samples are made of the anatase phase. However, when Mn ions are doped into TiO_2, manganese oxide such as MnO, Mn_2O_3, Mn_3O_4 and MnO_2 is not discovered, suggesting that the product is not a mixture of manganese oxide and TiO_2, and Mn ions have been inserted into the lattice of TiO_2. Since impurity ions could act as a strong barrier to the phase transition during calcination. Similar inhibition effects on the TiO_2 phase transition have been reported by other groups[22]. The effect of Mn doping on

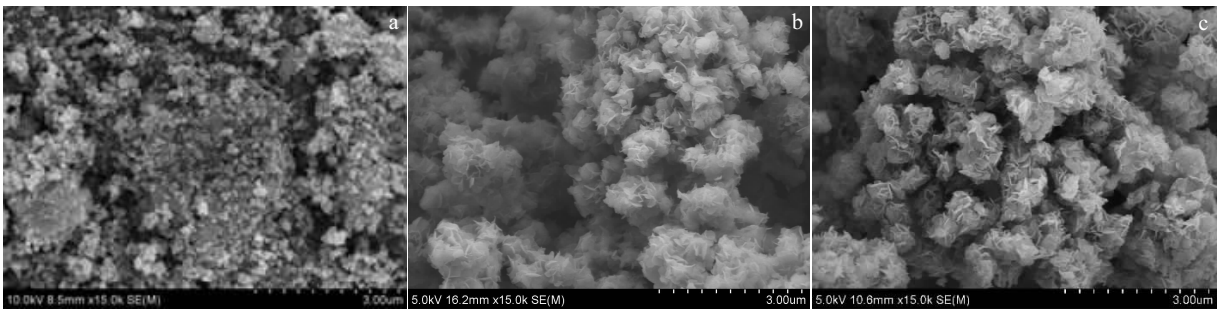

Fig.1 FESEM images of the synthesized TiO_2 PS (a), TiO_2 NS (b), and Mn-TiO_2 NS (c)

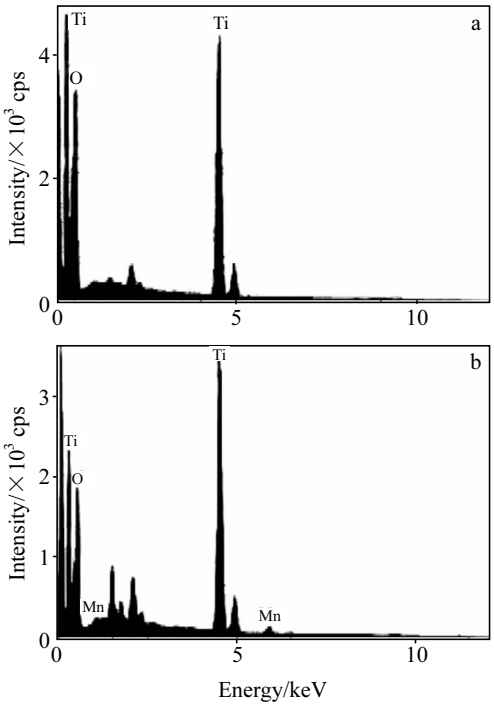

Fig.2 EDS spectra of the synthesized TiO_2 NS (a) and Mn-TiO_2 NS (b)

Table 1 EDS analysis of TiO_2 NS and Mn-TiO_2 NS (wt%)

Element	TiO_2 NS	Mn-TiO_2 NS
O	27.93	18.60
Ti	72.07	77.95
Mn	0	3.45
Total	100	100

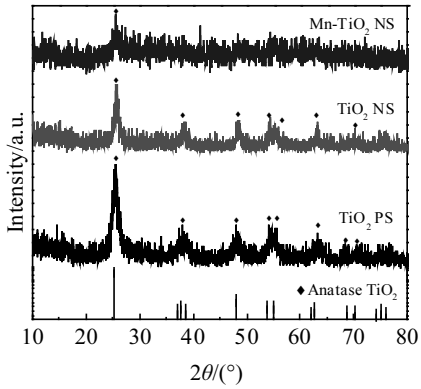

Fig.3 XRD patterns of the synthesized TiO_2 PS, TiO_2 NS and Mn-TiO_2 NS and standard anatase TiO_2

the microstructural change in nanocrystalline material was further studied by Raman spectra. According to literature data[25], anatase features in the Raman spectra has six Raman active modes: A_g, B_{g1}, B_{g2}, E_{g1}, E_{g2}, E_{g3} (519, 399, 519, 144, 197 and 639 cm^{-1}), as shown in Fig.4a. Among those active modes, the E_{g1}, E_{g2} and E_{g3} modes are important, since they are O-Ti-O bending type vibrations and sensitive to local oxygen vacancies.

Due to Mn doping, the structural is distorted, and it is expected that the phonon state of TiO_2 lattice will be disturbed moderately. The expanded view of this mode is shown in Fig.4b. The three modes of TiO_2 correspond to anatase TiO_2, which conforms to the result of XRD. Fig.4b demonstrates that the Raman E_{g1}, peak of Mn-TiO_2 blue shifted and widen in comparison with TiO_2 PS and TiO_2 NS. These changes in the Raman peak are caused by the transformation of the structure and the generation of defects on the lattice site of TiO_2 on Mn doping. From the above description, it can be speculated that titanium ion is partially replaced by manganese ion. Formation of the Mn-O bonds leads to the generation of defects on the lattice site of TiO_2 and oxygen vacancies. Meanwhile, the symmetry of O-Ti-O bond is destroyed, which makes the Raman peak intensity of Mn-TiO_2 NS weaken and E_{g1} and E_{g3} mode slightly shift.

According to Fig.2~Fig.4, manganese ions replace some titanium ions to generate a new structure, instead of the simple mixture manganese oxide and TiO_2.

In order to get more insights into the influence of the hydrothermal and doping processes on TiO_2 samples, nitrogen adsorption-desorption measurements were conducted to characterize the specific surface areas of TiO_2 PS, TiO_2 NS and Mn-TiO_2 NS. Fig.5 shows the adsorption and desorption isotherm curves. The isotherm curves of TiO_2 NS and Mn-

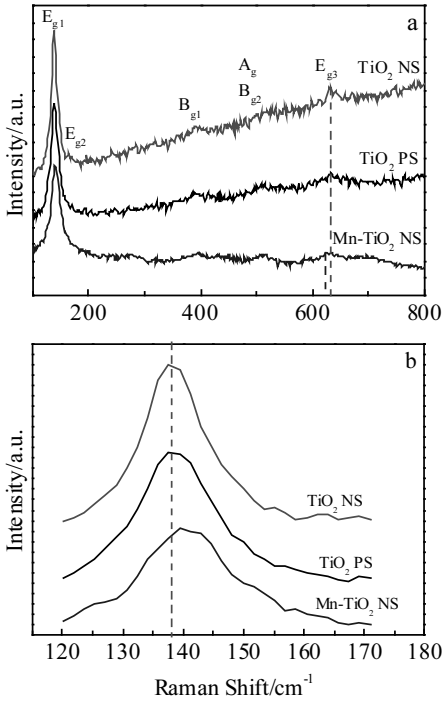

Fig.4 Raman spectra (a) and corresponding expanded view (b) of the synthesized TiO_2 PS, TiO_2 NS and Mn-TiO_2 NS

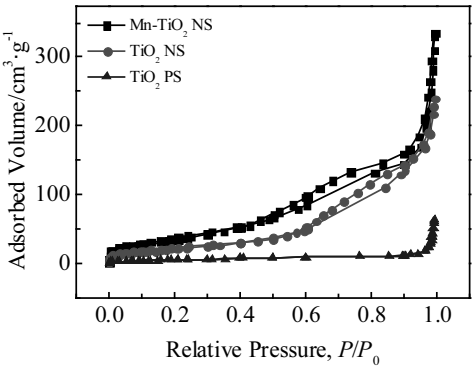

Fig.5 Nitrogen adsorption and desorption curves of TiO_2 PS, TiO_2 NS and Mn-TiO_2 NS

TiO_2 NS exhibit the typical adsorption hysteresis, indicating that these two samples are mesoporous structures. Their specific surface areas were calculated using the BJH method to be 83.2 and 149.0 $m^2 \cdot g^{-1}$, respectively. Both of the two samples have higher specific surface areas than TiO_2 PS (13.1 $m^2 \cdot g^{-1}$). Furthermore, Mn-TiO_2 NS has a larger specific surface area than TiO_2 NS. The Mn-TiO_2 NS and TiO_2 NS have the same structure but different specific surface area, because of the doping of manganese ions. The different valances of Mn increase the repulsive force between Mn-TiO_2 NS, and thus Mn-TiO_2 NS have a larger specific surface area than TiO_2 NS.

2.2 Electrochemical performance of catalysts

The electrochemical performance of pure KB, KB+TiO_2 PS, KB+TiO_2 NS and KB+Mn-TiO_2 NS electrode was further investigated in Li-air batteries. To study the catalytic activity of KB+Mn-TiO_2 NS electrode, CV tests (Fig.6) were carried out in a Li-air battery with the potential (vs Li/Li^+) varying from 2.0~4.5 V and a scan rate of 0.5 $mV \cdot s^{-1}$. Compared with pure KB, KB+TiO_2 PS and KB+TiO_2 NS electrodes, the KB+Mn-TiO_2 NS electrode delivers much higher oxygen reduction triggering onset potential and lower oxygen releasement onset voltage during the cathodic/anodic sweep. It can be attributed to the nanosheets structure and the amount of Mn associated with oxygen vacancies in the Mn-TiO_2 NS, which can increase the electronic conductivity and reduce kinetic barrier for ORR and OER process. Based on the above reason, it is expected that the nanosheets structure and the amount of Mn associated with oxygen vacancies in the Mn-TiO_2 NS may lead to a better catalytic activity for ORR/OER in non-aqueous Li-O_2 batteries.

Fig.7 shows that the EIS plots of the four kinds of Li-O_2 batteries in the air condition. Each curve consists of two parts, a small semicircle at the high-frequency region attributes to the charge-transfer resistance and a slope line at the low-frequency region associated with the ion diffusion process within the electrode[26]. The first crossing of semicircle and *X*-axis represents to the battery internal resistances, while the second represents to the interfacial resistance and charge transfer resistance. As shown in Fig.7, the KB+Mn-TiO_2 NS electrode presents the minimum internal resistances, interfacial resistance and charge transfer resistance. It demonstrates that the Mn-TiO_2 NS catalyst can improve the charge transfer efficiency in Li-air batteries, which is consistent with the CV result.

Fig.8 shows the first charge-discharge curve of the four kinds of electrodes measured between 2.20 and 4.5 V at a current density of 250 and 500 $mA \cdot g^{-1}$. The Li-air battery of the KB+Mn-TiO_2 NS electrode is the highest average discharge voltage plateau of about 2.66 and 2.58 V, which is higher than that of the pure KB electrode (2.60 and 2.48 V). In addition, The KB+Mn-TiO_2 NS electrode shows a much lower discharge and charge overpotential (1.24 V), and a much higher specific capacity (9374.23 $mAh \cdot g^{-1}$) than the KB (1719.35 $mAh \cdot g^{-1}$), KB+TiO_2 PS (5479.81 $mAh \cdot g^{-1}$) and KB+TiO_2 NS (5515.60 $mAh \cdot g^{-1}$) based Li-O_2 battery. It is referred that the Mn-TiO_2 NS electrode provides more active sites for chemical adsorption of oxygen and reduces the activation energy of oxygen reduction for Li-O_2 batteries.

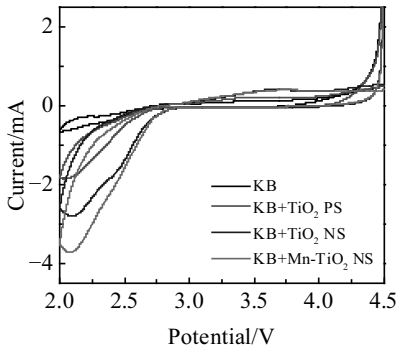

Fig.6 CV curves of KB, KB+TiO_2 PS, KB+TiO_2 NS and KB+Mn-TiO_2 NS cathodes at a scanning rate of 0.5 $mV \cdot s^{-1}$ in dry air atmosphere

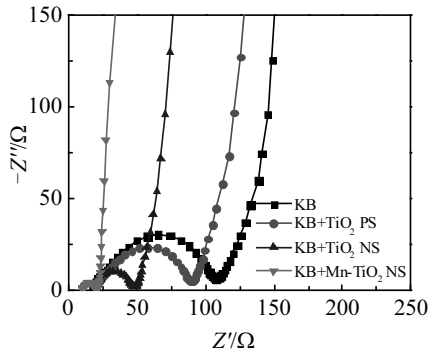

Fig.7 Nyquist plots of Li-air cells with KB, KB+TiO_2 PS, KB+TiO_2 NS and KB+Mn-TiO_2 NS cathodes under open circuit condition

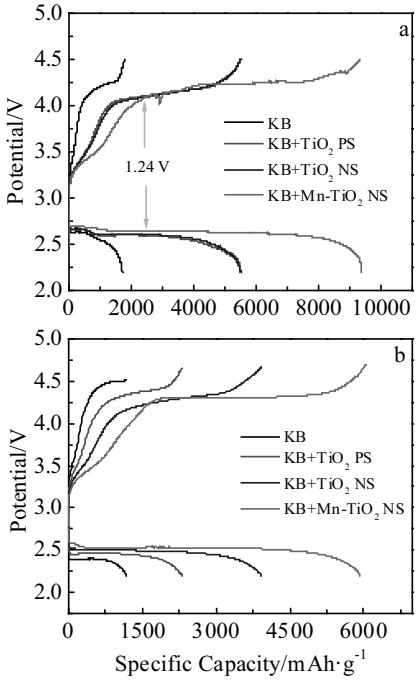

Fig.8 Initial discharge of Li-air cells with KB, KB+TiO_2 PS, KB+TiO_2 NS and KB+Mn-TiO_2 NS cathodes capacity measured at the current densities of 250 mA·g^{-1} (a) and 500 mA·g^{-1} (b)

2.3 Cycle performance and discharge product analysis

In Fig.9 and Fig.10, the cycling stability of the KB, KB+TiO_2 PS, KB+TiO_2 NS and KB+Mn-TiO_2 NS was manifested at the current density of 500 and 250 mA·g^{-1} with a fixed capacity of 1000 mAh·g^{-1}, and the KB+Mn-TiO_2 NS electrode demonstrates a favorable cycling performance for the Li-O_2 batteries. As shown in Fig.9, the discharge/charge terminal voltage for the KB+Mn-TiO_2 NS electrode remains stable 26 cycles (2.0 and 5.0 V), while for the other electrodes, their discharge terminal voltage drops quickly after 20 cycles. The Mn-TiO_2 NS electrode has a certain improvement in OER performance. This is consistent with what has been demonstrated by CV.

To give insights into the reaction mechanisms and clarify why the electrochemical performance of KB+Mn-TiO_2 NS electrode is superior to that of KB electrodes, the microstructures of discharged products of KB+Mn-TiO_2 NS and KB electrodes were investigated by FESEM. As shown in Fig.11, the fibrous material is an un-cleaned glass fiber diaphragm in FESEM image. After discharge, the KB electrode surface is covered with a layer of membrane. However, the discharge product is circular structure in the KB+Mn-TiO_2 NS electrode. It is inferred that KB+Mn-TiO_2 NS electrode adsorbs oxygen more easily than KB electrode for Li-O_2 batteries.

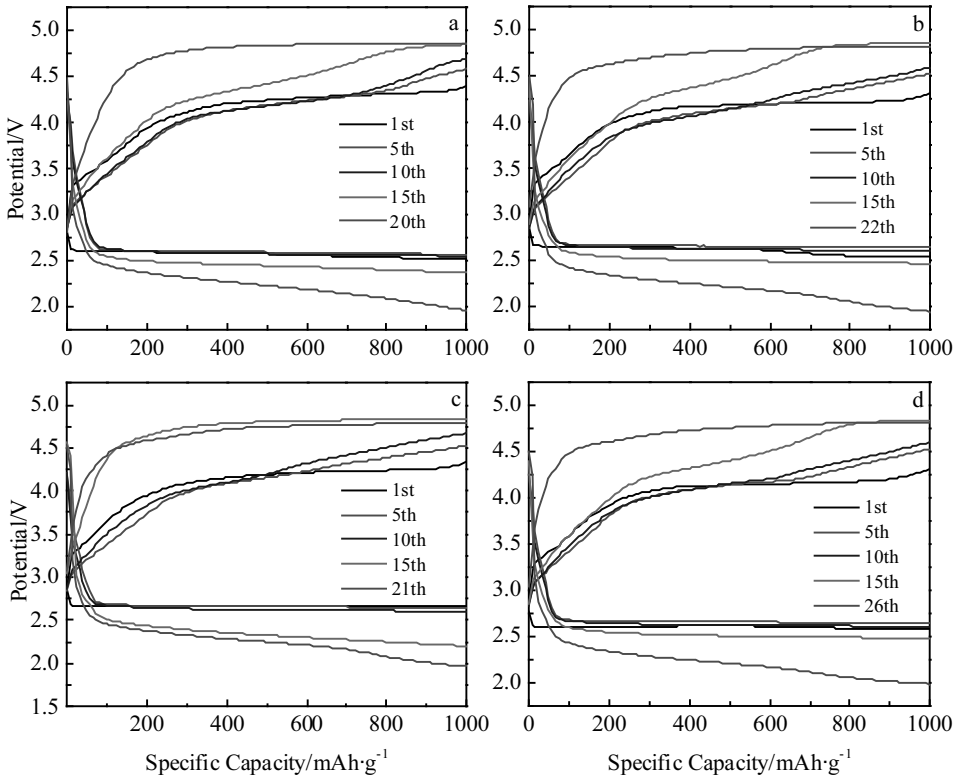

Fig.9 Voltage profiles for Li-O_2 batteries with KB (a), KB+TiO_2 PS (b), KB+TiO_2 NS (c), and KB+Mn-TiO_2 NS (d) electrodes cycled at a current density of 500 mA·g^{-1} and a fixed capacity of 1000 mAh·g^{-1}

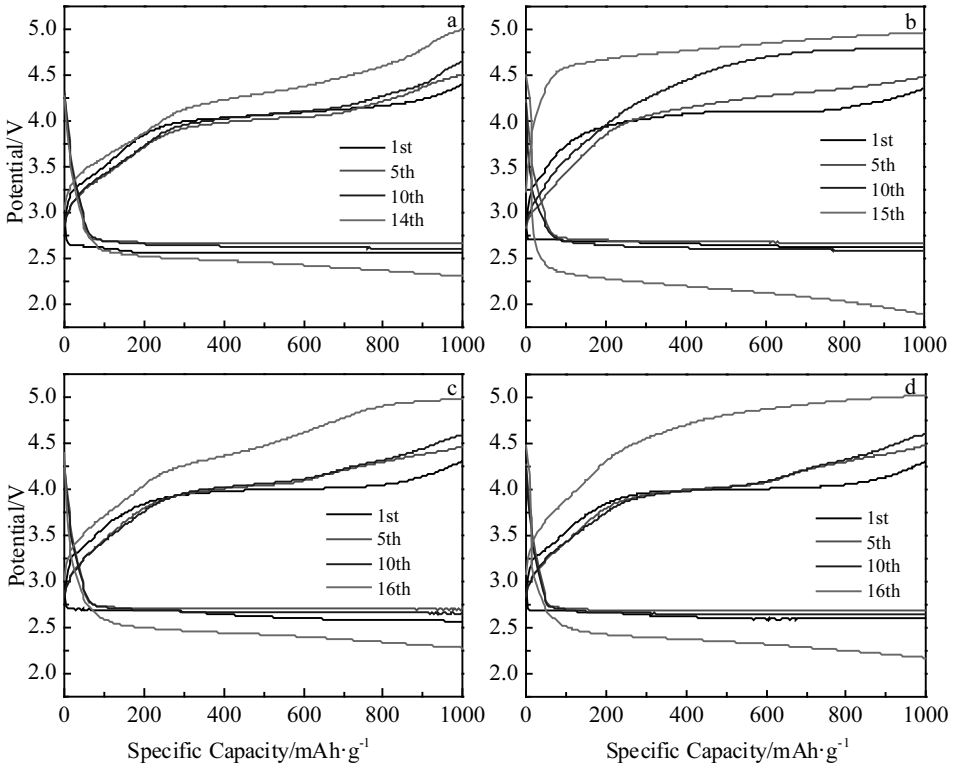

Fig.10 Voltage profiles for Li-O_2 batteries with KB (a), KB+TiO_2 PS (b), KB+TiO_2 NS (c), and KB+Mn-TiO_2 NS (d) electrodes cycled at a current density of 250 mA·g^{-1} and a fixed capacity of 1000 mAh·g^{-1}

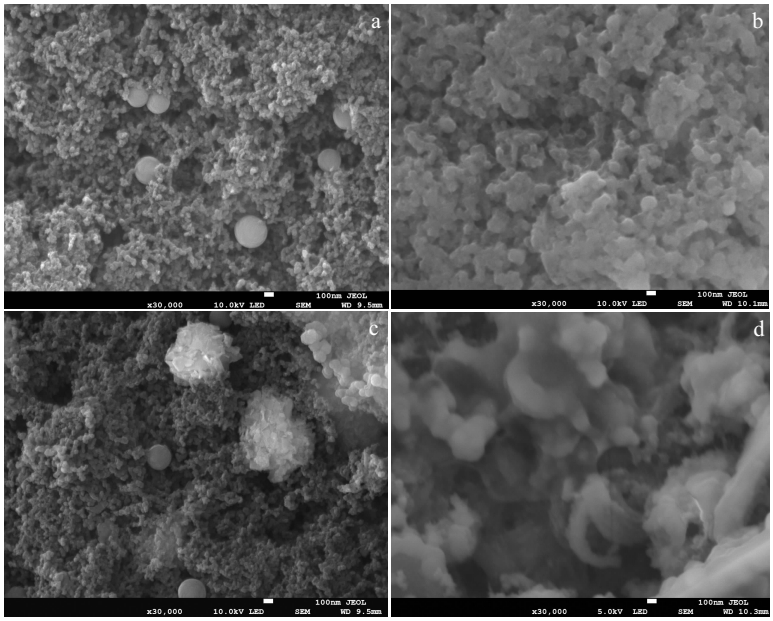

Fig.11 FESEM images of KB (a, b) and KB+Mn-TiO_2 NS (c, d) electrodes before (a, c) and after (b, d) discharge

3 Conclusions

1) Mn-TiO_2 was synthesized by a calcination treatment method and presented favorable catalytic activity towards both the ORR and the OER for nonaqueous Li-O_2 batteries. The assembled batteries employing Mn-TiO_2 NS as a catalyst deliver a high discharge capacity of 9374.23 mAh·g^{-1} at the current density of 250 mA·g^{-1}.

2) Mn-TiO_2 NS electrode has the largest specific surface area and the lowest charge transfer resistance among all the samples for Li-O_2 batteries. More importantly, the overpotential of Mn-TiO_2 NS electrode is lower than that of the TiO_2 NS and TiO_2 PS electrode for Li-O_2 batteries. Mn-TiO_2 NS electrode can not only facilitate continuous oxygen flow and charge transport during cycle, but also provide enough reaction sites for Li_2O_2 deposition and decomposition for Li-O_2 batteries. These results suggest that the Mn-TiO_2 NS catalyst is a promising material for Li-O_2 batteries or other energy storage devices.

References

1 Agyeman D A, Song K, Kang S H *et al*. *Journal of Materials Chemistry A*[J], 2015, 3(45): 22557
2 Giannuzzi R, Manca M, De Marco L *et al*. *ACS Applied Materials & Interfaces*[J], 2014, 6(3): 1933
3 Hong Z S, Hong J X, Xie C B *et al*. *Electrochimica Acta*[J], 2016, 202: 203
4 Hou C, Han J H, Liu P *et al*. *Nano Energy*[J], 2018, 47: 427
5 Kang S H, Song K, Jung J *et al*. *Journal of Materials Chemistry A*[J], 2014, 2(46): 19660
6 Leng L M, Li J, Zeng X Y *et al*. *Nanoscale*[J], 2018, 10(6): 2983
7 Li Y, Huang Y F, Zhang Z L *et al*. *Chemical Engineering Journal*[J], 2016, 283: 911
8 Lu F L, Wang Y R, Jin C *et al*. *Journal of Power Sources*[J], 2015, 293: 726
9 Luo C P, Li J D, Tong S F *et al*. *Chemical Communication*[J], 2018, 54(23): 2858
10 Meng F L, Chang Z W, Xu J J *et al*. *Materials Horizons*[J], 2018, 5: 298
11 Park J B, Belharouak I, Lee Y J *et al*. *Journal of Power Sources*[J], 2015, 295: 299
12 Park J B, Luo X Y, Lu J *et al*. *The Journal of Physical Chemistry C*[J], 2015, 119(27): 15036
13 Shao J Q, Song M Y, Wu G *et al*. *Energy Storage Materials*[J], 2018, 13: 57
14 Wang F, Li H J, Wu Q X *et al*. *Electrochimica Acta*[J], 2016, 202: 1
15 Wang L, Wang H Y, Wang Y *et al*. *Advanced Materials*[J], 2013, 25(45): 6539
16 Wang X H, Sun L M, Sun X L *et al*. *Materials Research Bulletin*[J], 2017, 96: 533
17 Wang Z Y, Chen X, Cheng Y H *et al*. *The Journal of Physical Chemistry C*[J], 2015, 119(46): 25684
18 Xu J J, Chang Z W, Yin Y B *et al*. *ACS Central Science*[J], 2017, 3(6): 598
19 Yang S X, He P, Zhou H S. *Energy Storage Materials*[J], 2018, 13: 29
20 Yang X Y, Xu J J, Chang Z W *et al*. *Advanced Energy Materials*[J], 2018, 8(12): 1702242
21 Yoon K R, Shin K, Park J *et al*. *ACS Nano*[J], 2018, 12(1): 128
22 Zhang P, Sun D F, He M *et al*. *Chem Sus Chem*[J], 2015, 8(11): 1972
23 Zhang Z, Chen Y N, Bao J *et al*. *Particle & Particle Systems Characterization*[J], 2015, 32(6): 680
24 Zhou W, Zhang H Z, Nie H J *et al*. *ACS Appl Mater Interfaces*[J], 2015, 7: 3389
25 Zhao G Y, Niu Y N, Zhang L *et al*. *Journal of Power Sources*[J], 2014, 270: 386
26 Zhao W, Li X M, Yin R *et al*. *Nanoscale*[J], 2018, 11: 50

锰掺杂二氧化钛纳米片为正极催化剂制备高性能锂空气电池

王泓蛟，王　慧，曹慧群，罗仲宽，王　芳

(深圳大学，广东 深圳 518060)

摘　要：使用 Mn 掺杂的 TiO_2 纳米片（Mn-TiO_2 纳米片）作为阴极催化剂来改善锂-空气电池的电化学性能。首先，通过简单的水热方法处理煅烧过的金红石制备 Mn-TiO_2 纳米片；其次，将聚偏氟乙烯(PVDF)溶于 N-甲基-2-吡咯烷酮(NMP)溶剂中，然后将 KB 和 Mn-TiO_2 纳米片与 PVDF/NMP 溶液混合，制备正极悬浮液。最后，将正极悬浮液涂覆到碳纸上(直径 15 mm)，并在 60 ℃烘箱里烘干 3 h，获得 Mn-TiO_2 纳米片正极。正如预期，在 250 $mA·g^{-1}$ 的电流密度下，KB 和 Mn-TiO_2 纳米片作为锂-空气电池的电极表现出较低的过电势（1.24 V）和较高的放电容量（9374.23 $mAh·g^{-1}$）。这表明 Mn-TiO_2 纳米片作为锂空气电池正极催化剂具有极大的应用前景。

关键词：Mn-TiO_2 纳米片；催化效应；KB；高性能；锂空气电池

作者简介：王泓蛟，男，1994 年生，硕士，深圳大学化学与环境工程学院，广东 深圳 518060，电话：0755-26557381，E-mail: 1725546029@qq.com